Japanese Journal of Applied Physics
Vol. 43, No. 6A, 2004, pp. L731–L734

Electronic Structure of Protonic Conductor $BaCe_{0.90}Y_{0.10}O_{3-\delta}$ Probed by Soft-X-Ray Spectroscopy

Tohru HIGUCHI, Hiroshige MATSUMOTO[1], Tetsuo SHIMURA[2], Keiji YASHIRO[1], Tatsuya KAWADA[1], Junichiro MIZUSAKI[1], Shik SHIN[3,4] and Takeyo TSUKAMOTO

Department of Applied Physics, Tokyo University of Science, Tokyo 162-8601, Japan
[1] *Institute of Multidisciplinary Research for Advanced Materials, Tohoku University, Sendai 980-8577, Japan*
[2] *Center for Integrated Research in Science and Engineering, Nagoya University, Nagoya 464-8603, Japan*
[3] *Institute for Solid State Physics, University of Tokyo, Chiba 277-8581, Japan*
[4] *RIKEN, Hyogo 679-5198, Japan*

(Received March 2, 2004; accepted April 2, 2004; published May 21, 2004)

The electronic structure of the protonic conductor Y-doped $BaCeO_3$ ($BaCe_{0.90}Y_{0.10}O_{3-\delta}$) has been studied by photoemission spectroscopy and X-ray absorption spectroscopy. The Fermi level (E_F) of H_2-annealed $BaCe_{0.90}Y_{0.10}O_{3-\delta}$ shifts to the conduction band side by approximately 0.4 eV. The holes and acceptor level are observed at the top of the valence band and just above E_F, respectively. Their intensities are lower in the H_2-annealed $BaCe_{0.90}Y_{0.10}O_{3-\delta}$, indicating that doped hydrogen enters hole and acceptor states. These findings indicate that the electronic structure of the protonic conductor $BaCe_{0.90}Y_{0.10}O_{3-\delta}$ obeys the rigid-band model. [DOI: 10.1143/JJAP.43.L731]

KEYWORDS: $BaCe_{0.90}Y_{0.10}O_{3-\delta}$, photoemission spectroscopy (PES), electronic structure, X-ray absorption spectroscopy (XAS), rigid-band model, Ce-O hybridization

Perovskite-type oxide $BaCeO_3$ exhibits appreciable proton conduction under hydrogen-containing atmosphere at high temperature when trivalent cation is substituted into the Ce^{4+} site.[1–10] This protonic conductor is expected as a solid electrolyte for high-temperature electrochemical devices such as hydrogen sensor and hydrogen fuel cell. In particular, Y^{3+}-doped $BaCeO_3$ ($BaCe_{1-x}Y_xO_{3-\delta}$) has not only the highest conductivity (1.2×10^{-1} S·cm^{-1} in dry air and 6.7×10^{-2} S·cm^{-1} in wet hydrogen at 1000°C),[5] but also the high chemical stability at the high-temperature region. Many experimental investigations into the mechanism of proton migration have been reported for $BaCeO_3$.[4–14] On the other hand, understanding the electronic structure is also one of the most important subjects for further applications.

The electronic structures of perovskite-type protonic conductors have been studied using photoemission spectroscopy (PES) and X-ray absorption spectroscopy (XAS).[15–19] For many protonic conductors such as $CaZrO_3$, $SrTiO_3$ and $SrCeO_3$, the Fermi levels (E_F) of dry-annealed conductors are located at the valence band side. The E_F is higher in H_2-annealed conductors, indicating the existence of hydrogen that acts as a positive charge. In the O 1*s* XAS spectra of dry-annealed conductors, the hole state and acceptor-induced level are observed at the top of the valence band and just above E_F, respectively. The intensities of hole state and acceptor-induced level decrease and the hydrogen-induced level is created at just below E_F in H_2-annealed conductors. These findings are the effect of the hydrogen doping of the electronic structure expected from the rigid-band model. Similar phenomena might be expected in $BaCe_{1-x}Y_xO_{3-\delta}$. However, the electronic structure has not been clarified thus far.

In this study, the electronic structure of the protonic conductor $BaCe_{0.90}Y_{0.10}O_{3-\delta}$ has been studied using PES and XAS techniques. The PES spectra reflect the electronic structure in the occupied state. The XAS spectra, which have a clear selection rule regarding the angular momentum due to dipole transition, reflect the electronic structure of unoccupied state. Thus, we observe the shift of E_F and impurity state in the band gap region expected from rigid-band model, as was previously reported in the cases of $CaZrO_3$, $SrTiO_3$ and $SrCeO_3$.[15–19]

$BaCe_{0.90}Y_{0.10}O_{3-\delta}$ samples were sintered ceramics prepared by the solid state reaction of $BaCO_3$, CeO_2, and Y_2O_3 at 1350°C, and pressed into cylinders of ϕ10 mm × 5 mm, then sintered again in air at 1650°C for 10 h; the sample at this stage reflects an oxidative atmosphere and is below referred to as air-annealed sample. After the sintering, another sample was treated in an atmosphere of wet 1% H_2 (diluted by Ar; water vapor pressure was 1.9×10^3 Pa) at 800°C for 10 h. The latter reflects a wet-reducing atmosphere and is below expressed as H_2-annealed sample. These samples were confirmed as having a single phase with a perovskite structure by powder X-ray diffraction analysis.

PES and XAS measurements were carried out at the revolver undulator beamline BL-19B at the Photon Factory of the High Energy Accelerator Organization, Tsukuba, Japan. Synchrotron radiation was monochromatized using a varied-line spacing plane grating whose average groove density is 1000 lines/mm. The PES spectra were measured by an electrostatic hemispherical analyzer whose radius is 100 mm. The XAS spectra were measured using a Si photodiode. The samples were scraped in situ with a diamond file in a vacuum of 3.0×10^{-10} Torr in order to obtain a clean surface. The total-energy resolutions of PES and XAS were approximately 40 meV and 100 meV, respectively. The energy axis was calibrated by measuring the 4*f* core level of Au film.

Figure 1 shows the PES spectra in the (a) valence band and (b) O 1*s* core level energy regions of air-annealed and H_2-annealed $BaCe_{0.90}Y_{0.10}O_{3-\delta}$. These PES spectra are normalized by the beam current and measurement time. The Fermi level (E_F) of air-annealed $BaCe_{0.90}Y_{0.10}O_{3-\delta}$ is located at ~0.6 eV above the top of the valence band. The positions of the valence band and O 1*s* core level are shifted to higher binding energy by 0.4 eV in H_2-annealed $BaCe_{0.90}Y_{0.10}O_{3-\delta}$. These shifts mean that E_F becomes higher in H_2-annealed $BaCe_{0.90}Y_{0.10}O_{3-\delta}$, indicating the effect of the hydrogen doping on the rigid-band model.[16]

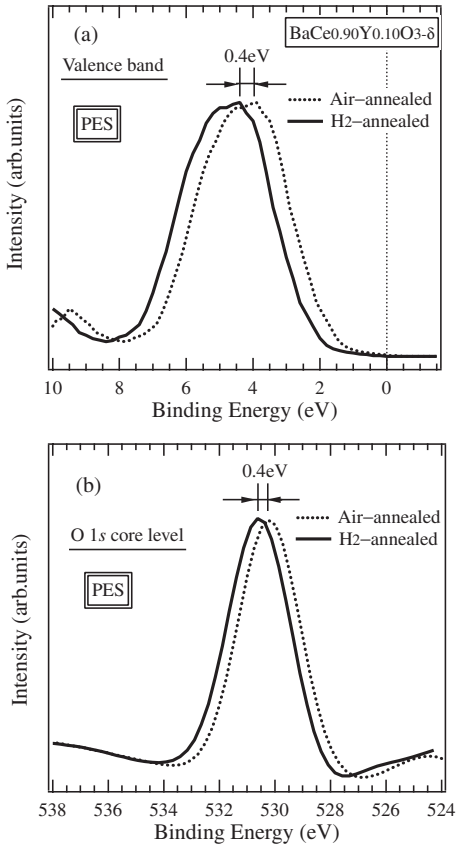

Fig. 1. Comparisons of the PES spectra in the (a) valence band and (b) O 1*s* core level regions between air-annealed and H_2-annealed $BaCe_{0.90}Y_{0.10}O_{3-\delta}$. The PES spectra in the valence band and O 1*s* core level were measured at $h\nu = 117$ eV and 800 eV, respectively.

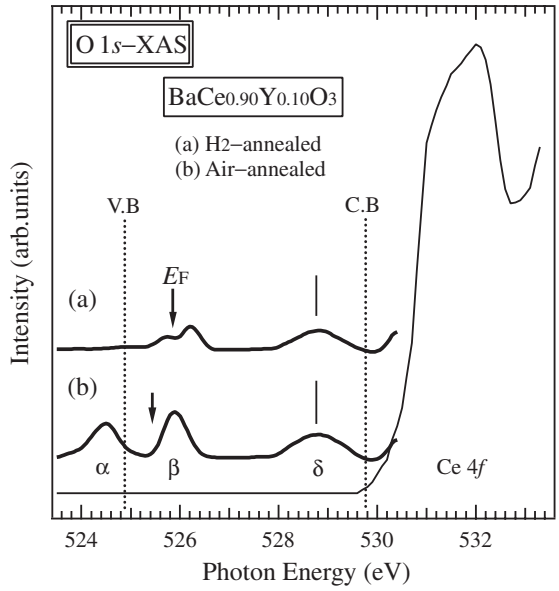

Fig. 2. O 1*s* XAS spectra of air-annealed and H_2-annealed $BaCe_{0.90}Y_{0.10}O_{3-\delta}$. The intensity of the photon energy region below 530 eV is expanded and shown as a thick line.

Figure 2 shows the O 1*s* XAS spectra of air-annealed and H_2-annealed $BaCe_{0.90}Y_{0.10}O_{3-\delta}$. The O 1*s* XAS spectra are normalized by the Ba 5*d* peak of the conduction band, although the peak is not shown in this figure. From the dipole selection rule, it is understood that the O 1*s* XAS spectra of Ce oxides correspond to transitions from O 1*s* to the O 2*p* character.[19] The large band around 532 eV is mainly composed of the O 2*p* state hybridized with the unoccupied Ce 4*f* state. The spectral intensity below the threshold is expanded by ten times and is shown as a thick line above the XAS spectrum in order to show the electronic structure in the band gap energy region. The XAS features below E_F correspond to the thermal excited structure from the valence band. An arrow shows the top of the valence band. In both samples, the energy separation between E_F and the top of the valence band correlates with the results shown in Fig. 1(a).

In air-annealed $BaCe_{0.90}Y_{0.10}O_{3-\delta}$, three features denoted by the α, β, and δ peaks are observed in the band gap energy region. The feature δ is considered to be a defect-induced level of the Ce 4*f* state, since the feature is located at the bottom of the Ce 4*f* conduction band. The same defect-induced level has been reported in $SrCe_{1-x}Y_xO_{3-\delta}$.[19] The feature α is assigned to holes created by Y^{3+} doping at the top of the valence band, which is mainly composed of nonbonding O 2*p* states in the valence band. In the absorption spectra in the vacuum ultraviolet region, the authors have clarified that the band gap of $SrCe_{1-x}Y_xO_{3-\delta}$ increases with increasing Y^{3+} concentration.[20] The increasing the band gap contributes to the presence of holes created at the top of the valence band. The existence of holes has been observed in the O 1*s* XAS spectra of $SrCe_{1-x}Y_xO_{3-\delta}$.[19] Such a situation is also expected in $BaCe_{0.90}Y_{0.10}O_{3-\delta}$. This finding indicates that the filling of the acceptor is rigid-bandlike. The feature β at E_F is assigned to the acceptor level, since it lies just above E_F. In H_2-annealed $BaCe_{0.90}Y_{0.10}O_{3-\delta}$, the hole states are absent and the intensities of acceptor and Ce 4*f* defect-induced level decrease. These behaviors indicate that doped hydrogen enters the hole at the top of the valence band, acceptor, and Ce 4*f* defect-induced level. A new feature just below E_F of H_2-annealed $BaCe_{0.90}Y_{0.10}O_{3-\delta}$ is considered to be a hydrogen-induced level. The existences of holes, acceptor, and hydrogen-induced levels are expected from the rigid- band model.

Figure 3(a) shows the Ce $4d \rightarrow 4f$ XAS spectrum of air-annealed $BaCe_{0.90}Y_{0.10}O_{3-\delta}$. The overall profile is similar to the XAS spectra of CeO_2 and $SrCeO_3$.[18,21] The vertical bars, which are labeled as on and off, indicate the selected photon energies for the resonant-PES (RPES) measurements.

Figure 3(b) shows the RPES spectra in the Ce $4d \rightarrow 4f$ energy region of $BaCe_{0.90}Y_{0.10}O_{3-\delta}$. The binding energy of air-annealed $BaCe_{0.90}Y_{0.10}O_{3-\delta}$ is shifted to higher binding energy by 0.4 eV in order to compare the line shape of H_2-annealed $BaCe_{0.90}Y_{0.10}O_{3-\delta}$. The off-resonance spectra have three features denoted by the A, B and C peaks, which mainly consist of the O 2*p* states. The band width of $BaCe_{0.90}Y_{0.10}O_{3-\delta}$ is in agreement with that of $SrCe_{0.90}Y_{0.05}O_{3-\delta}$ which has the same crystalline structure as $BaCe_{0.90}Y_{0.10}O_{3-\delta}$. In both on-resonance spectra, the intensity of the feature B is resonantly enhanced by the Ce $4d \rightarrow 4f$ excitation. The resonance effect is stronger in H_2-annealed $BaCe_{0.90}Y_{0.10}O_{3-\delta}$. However, the features A and C do not exhibit the resonance effect.

Figure 3(c) shows the difference spectra by subtracting the off-resonance spectra from the on-resonance spectra. The

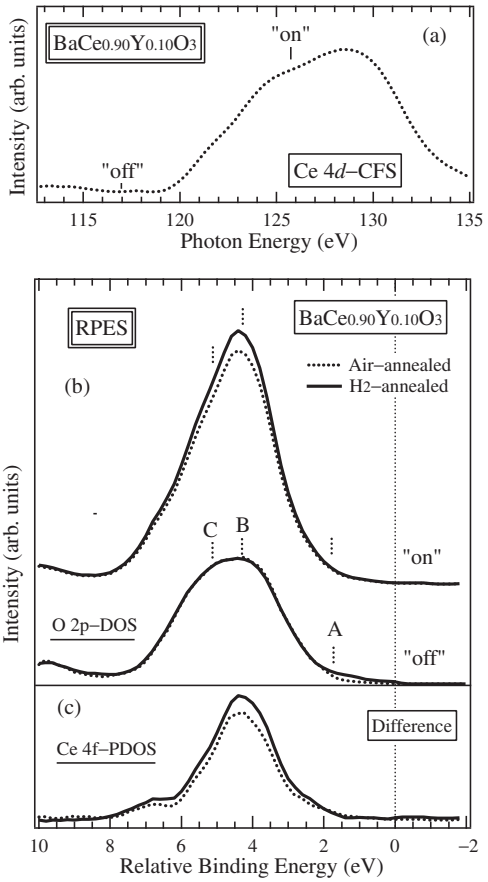

Fig. 3. (a) CFS spectrum of air-annealed $BaCe_{0.90}Y_{0.10}O_{3-\delta}$, corresponding to the Ce $4d \rightarrow 4f$ giant absorption spectrum. (b) On- and off-resonance spectra of air-annealed and H_2-annealed $BaCe_{0.90}Y_{0.10}O_{3-\delta}$. The on- and off-resonance spectra were measured at $h\nu = 125$ eV and 117 eV, respectively. (c) Difference spectra obtained by subtracting the off-resonance spectra from the on-resonance spectra.

difference spectra correspond to the Ce $4f$ partial density of state (PDOS) in the valence band. The Ce $4f$ contribution is more significant in the feature B, where the O $2p$ states have a larger admixture of Ce $4f$ states. The feature C corresponds to O $2p$ states, which are not hybridized with Ce derived states. Such a situation has been reported in CeO_2 and $SrCeO_3$.[18,21–23] Therefore, the valence states originating from the O $2p$ states are hybridized with the Ce $4f$ states. By comparing each difference spectrum, the Ce $4f$ PDOS is seen to be larger in the case of H_2-annealed $BaCe_{0.90}Y_{0.10}O_{3-\delta}$. This implies that the hybridization effect between the Ce $4f$ state and O $2p$ state becomes more extensive with hydrogen doping, indicating that the bond length between Ce^{4+} and O^{2-} ions or the symmetry changes with hydrogen doping.[18]

The feature A is observed at the top of the valence band of H_2-annealed $BaCe_{0.90}Y_{0.10}O_{3-\delta}$, although there is no structure at the top of the valence band of air-annealed $BaCe_{0.90}Y_{0.10}O_{3-\delta}$. The energy position correlates with the hole state (feature α) in Fig. 2. The existence of the feature A has been observed in the RPES spectra of undoped $SrCeO_3$ and CeO_2.[21–23] The Ce ion in $BaCeO_3$ is nominally tetravalent with no $4f$ electron such as $SrCeO_3$. In the constant-initial state spectra of CeO_2 and $SrCeO_3$, it has been reported that the valence band consists of mixed-valent state between the $4f^0$ and $4f^1\underline{L}$ configurations in the ground state. Here, $\underline{L}$ denotes the hole in the valence band mainly composed of the O $2p$ state. Such a situation can be also expected in $BaCe_{0.90}Y_{0.10}O_{3-\delta}$. Therefore, we ascribe the feature B to correspond to the $4f^0$ (Ce^{4+}) state and the feature A to correspond to the $4f^1\underline{L}$ (Ce^{3+}) state. With a simple consideration, the hybridization between the $4f^0\underline{L}$ and $4f^1\underline{L}^2$ configurations in the final state is expected to nearly equal that between the $4f^0$ and $4f^1\underline{L}$ configurations in the ground state with the average $4f$ electron number of approximately 0.5. The average $4f$ electron number might change with hydrogen concentration. Thus, the increase in the intensity of the feature A for H_2-annealed $BaCe_{0.90}Y_{0.10}O_{3-\delta}$ indicates that the doped hydrogen exchanges with the $4f^1\underline{L}$ (Ce^{3+}) state.

In conclusion, the electronic structure of the protonic conductor $BaCe_{0.90}Y_{0.10}O_{3-\delta}$ was studied by XAS and PES. The valence band is composed of the O $2p$ states hybridized with Ce $4f$ states. E_F of H_2-annealed $BaCe_{0.90}Y_{0.10}O_{3-\delta}$ shifts to the conduction band by 0.4 eV. In air-annealed $BaCe_{0.90}Y_{0.10}O_{3-\delta}$, the holes and acceptor level are observed at the top of the valence band and just above E_F, respectively. In H_2-annealed $BaCe_{0.90}Y_{0.10}O_{3-\delta}$, the hole states are absent and the intensities of acceptor and Ce $4f$ defect-induced level decrease, indicating that the doped hydrogen exchanges with the hole at the top of the valence band, which corresponds to the $4f^1\underline{L}$ (Ce^{3+}) state. These findings show the effect of the hydrogen doping on the rigid-band model.

This work was partially supported by New Energy and Industrial Technology Development Organization (NEDO), and the Foundation for Materials Science and Technology of Japan (MST Foundation).

1) H. Iwahara, T. Esaka, H. Uchida and N. Maeda: Solid State Ionics **3/4** (1981) 359.
2) S. Shin, H. H. Huang, M. Ishigame and H. Iwahara: Solid State Ionics **40/41** (1990) 910.
3) H. Iwahara, H. Uchida, K. Kondo and K. Ogaki: J. Electrochem. Soc. **135** (1988) 529.
4) H. Matsumoto, S. Hamajima and H. Iwahara: J. Electrochem. Soc. **148** (2001) D121.
5) G. Ma, T. Shimura and H. Iwahara: Solid State Ionics **110** (1998) 103.
6) A. Mineshige, S. Okada, K. Sakai, M. Kobune, S. Fujii, H. Matsumoto, T. Shimura, H. Iwahara and Z. Ogumi: Solid State Ionics **162–163** (2003) 41.
7) H. Matsumoto, M. Okubo, S. Hamajima, K. Katahira and H. Iwahara: Solid State Ioncis **152–153** (2002) 715.
8) H. Matsumoto, S. Hamajima and H. Iwahara: Solid State Ionics **145** (2001) 25.
9) H. Iwahara, H. Matsumoto and K. Takeuchi: Solid State Ionics **136–137** (2000) 133.
10) H. Matsumoto, F. Asakura, K. Takeuchi and H. Iwahara: Solid State Ionics **129** (2000) 209.
11) S. Yamaguchi and N. Yamada: Solid State Ionics **162–163** (2003) 23.
12) K. S. Knight: Solid State Ionics **140** (2001) 18.
13) K. S. Knight: Solid State Ionics **74** (1994) 109.
14) F. Genet, S. Loridant, C. Ritter and G. Lucazeau: Solid State Ionics **60** (1999) 2009.
15) T. Higuchi, T. Tsukamoto, N. Sata, M. Ishigame, Y. Tezuka and S. Shin: Phys. Rev. B **57** (1998) 6978.
16) T. Higuchi, T. Tsukamoto, Y. Tezuka, K. Kobayashi, S. Yamaguchi and S. Shin: Jpn. J. Appl. Phys. **39** (2000) L133.
17) S. Yamaguchi, K. Kobayashi, T. Higuchi, S. Shin and Y. Iguchi: Solid State Ionics **136–137** (2000) 305.

18) T. Higuchi, T. Tsukamoto, S. Yamaguchi, N. Sata, M. Ishigame and S. Shin: Jpn. J. Appl. Phys. **42** (2003) 3526.
19) T. Higuchi, S. Yamaguchi, N. Sata, S. Shin and T. Tsukamoto: Jpn. J. Appl. Phys. **42** (2003) L1265.
20) T. Higuchi, N. Sata, S. Shin and T. Tsukamoto: in preparation for publication.
21) M. Matsumoto, K. Soda, K. Ichikawa, Y. Taguchi, K. Jouda, M. Kageyama, S. Tanaka, N. Sata, Y. Tezuka, S. Shin and O. Aita: J. Electr. Relat. Phenomn. **78** (1996) 179.
22) A. Fujimori: Phys. Rev. B **28** (1983) 2281.
23) E. Wuilloud, B. Delley, W.-D. Schneider and Y. Baer: Phys. Rev. Lett. **53** (1984) 202.